

1 **Transcranial Blood–Brain Barrier Opening in Alzheimer’s** 2 **Disease Patients Using a Portable Focused Ultrasound System** 3 **with Real-Time 2-D Cavitation Mapping**

4 Sua Bae^{1†}, Keyu Liu^{1†}, Antonios N. Pouliopoulos^{1†}, Robin Ji¹, Sergio Jiménez-Gambín¹, Omid Yousefian¹,
5 Alina R. Kline-Schoder¹, Alec J. Batts¹, Fotios N. Tsitsos¹, Danae Kokossis², Akiva Mintz³, Lawrence S.
6 Honig⁴, and Elisa E. Konofagou^{1,3*}

7 [†]These authors contributed equally to this work.

8 **Abstract**

9 **Background:** Focused ultrasound (FUS) in combination with microbubbles has recently shown great
10 promise in facilitating blood-brain barrier (BBB) opening for drug delivery and immunotherapy in
11 Alzheimer’s disease (AD). However, it is currently limited to systems integrated within the MRI
12 suites or requiring post-surgical implants, thus restricting its widespread clinical adoption. In this
13 pilot study, we investigate the clinical safety and feasibility of a portable, non-invasive
14 neuronavigation-guided FUS (NgFUS) system with integrated real-time 2-D microbubble cavitation
15 mapping.

16 **Methods:** A phase 1 clinical study with mild to moderate AD patients (N=6) underwent a single
17 session of microbubble-mediated NgFUS to induce transient BBB opening (BBBO). Microbubble
18 activity under FUS was monitored with real-time 2-D cavitation maps and dosing to ensure the
19 efficacy and safety of the NgFUS treatment. Post-operative MRI was used for BBB opening and
20 closure confirmation as well as safety assessment. Changes in AD biomarker levels in both blood
21 serum and extracellular vesicles (EVs) were evaluated, while changes in amyloid-beta (A β) load in
22 the brain were assessed through ¹⁸F-Florbetapir PET.

23 **Results:** BBBO was achieved in 5 out of 6 subjects with an average volume of 983 \pm 626 mm³
24 following FUS at the right frontal lobe both in white and gray matter regions. The outpatient
25 treatment was completed within 34.8 \pm 10.7 min. Cavitation dose significantly correlated with the
26 BBBO volume ($R^2 > 0.9$, $N=4$), demonstrating the portable NgFUS system’s capability of predicting
27 opening volumes. The cavitation maps co-localized closely with the BBBO location, representing
28 the first report of real-time transcranial 2-D cavitation mapping in the human brain. Larger opening

29 volumes correlated with increased levels of AD biomarkers, including A β 42 ($R^2=0.74$), Tau
30 ($R^2=0.95$), and P-Tau181 ($R^2=0.86$), assayed in serum-derived EVs sampled 3 days after FUS ($N=5$).
31 From PET scans, subjects showed a lower A β load increase in the treated frontal lobe region
32 compared to the contralateral region. Reduction in asymmetry standardized uptake value ratios
33 (SUVR) correlated with the cavitation dose ($R^2>0.9$, $N=3$). Clinical changes in the mini-mental state
34 examination over 6 months were within the expected range of cognitive decline with no additional
35 changes observed as a result of FUS.

36 **Conclusion:** We showed the safety and feasibility of this cost-effective and time-efficient portable
37 NgFUS treatment for BBBO in AD patients with the first demonstration of real-time 2-D cavitation
38 mapping. The cavitation dose correlated with BBBO volume, a slowed increase in pathology, and
39 serum detection of AD proteins. Our study highlights the potential for accessible FUS treatment in
40 AD, with or without drug delivery.

41 **Keywords:** Alzheimer’s disease; blood–brain barrier; focused ultrasound; microbubbles; cavitation
42 mapping;

43

44 **Author affiliations:**

45 ¹Department of Biomedical Engineering, Columbia University, New York, NY 10032, USA

46 ²Department of Radiation Oncology, Columbia University Irving Medical Center, New York, NY
47 10032, USA

48 ³Department of Radiology, Columbia University Irving Medical Center, New York, NY 10032, USA

49 ⁴Department of Neurology and Taub Institute, Columbia University Irving Medical Center 10032,
50 New York, NY, USA

51 Correspondence to: Sua Bae, Elisa E. Konofagou

52 Full address: 630 West 168th Street, New York, NY 10032, USA

53 E-mail: sb4495@columbia.edu, ek2191@columbia.edu

54

55 **Main Text**

56 **Introduction**

57 Alzheimer's disease (AD) is the most common neurodegenerative disorder, typically with
58 progressive amnesic cognitive impairment, and its prevalence increases with the aged population
59 growth [1]. Only since 2021 have effective disease-modifying treatments been available for
60 Alzheimer's disease. Currently, three monoclonal antibodies against amyloid-beta ($A\beta$) have been
61 shown to be effective: aducanumab [2], lecanemab [3], and donanemab [4]. Clinical studies have
62 demonstrated that administration of these antibodies markedly reduces the amount of $A\beta$ -containing
63 cerebral neuritic plaques, and the latter two antibodies have been proven to slow the clinical decline.
64 However, these antibodies do have limitations, including only limited slowing of cognitive decline
65 and cerebral side effects, such as amyloid-related imaging abnormalities of edema/effusion and
66 hemorrhage. Anti- $A\beta$ monoclonal antibodies bind to different forms of $A\beta$ and promote clearance
67 of plaques from the brain. However, for most, but not all, antibodies, the blood-brain barrier (BBB)
68 poses a challenge to their use because only a small proportion of the administered drug is able to
69 enter the brain, which affects their effectiveness in terms of dosage, frequency, and duration of
70 treatment [5,6]. Although direct intracerebral infusion could possibly circumvent the BBB
71 restriction, this invasive procedure entails risks [7].

72 Transient BBB opening by microbubble-mediated focused ultrasound (FUS) is a promising non-
73 invasive therapy for enhancing BBB permeability, thereby facilitating the delivery of therapeutic
74 drugs or promoting immune responses without the use of drugs [8–10]. In this treatment,
75 microbubbles are systemically administered while FUS induces the rapid oscillation of
76 microbubbles, called cavitation, at a targeted volume in the brain (Figure 1). Precise FUS treatment
77 can induce local and transient BBB opening (BBBO) and promote immune response [11,12].
78 Numerous preclinical studies have proven that BBBO can lead to a decrease in $A\beta$ or tau proteins in
79 the brain and the cognitive improvement with and without drugs by increased immune response such
80 as microglial phagocytosis [13–15].

81 Many clinical trials have demonstrated that magnetic resonance (MR)-guided focused ultrasound
82 (MRgFUS) can safely and transiently open BBB in patients with AD [16–19], amyotrophic lateral
83 sclerosis [20], Parkinson's disease [21], glioma [22,23], and brain metastases [24]. Previous studies
84 with AD patients have shown that BBBO induces a modest reduction in ^{18}F -Florbetaben uptake ratio

85 in PET with no cognitive worsening after multiple sessions of MRgFUS treatment [16–19,25]. A
86 recent study utilizing MRgFUS reported that monthly BBBO treatment combined with aducanumab
87 infusion led to a substantial reduction in A β levels in three patients over six months, as measured by
88 PET [26]. While MRgFUS is the most widely used approach for clinical trials of BBBO, it generally
89 requires the patient to stay still with their heads fixed by a stereotaxic frame in the MR scanner for
90 a few hours. Alternatively, an implantable FUS device has been utilized in clinical trials,
91 demonstrating a non-significant reduction in amyloid based on ^{18}F -Florbetapir PET scans after
92 multiple treatments [27]. Although this approach has been proven well-tolerated, it requires a burr
93 hole achieved with brain surgery, making it invasive. The invasiveness of the procedure makes it a
94 less preferred option for treating Alzheimer’s disease, particularly given that the typical patient
95 population is older and may have multiple comorbidities.

96 Given the need for repetitive treatments and the advanced age of Alzheimer’s disease patients, there
97 is a compelling demand for facilitating a low-cost and non-invasive treatment approach. Portable
98 neuronavigation-guided FUS (NgFUS) systems can provide FUS treatment outside an MR scanner
99 in an outpatient room. Portable systems have been employed in both preclinical and clinical studies
100 [28–31], but only one clinical study has been reported in the context of Alzheimer’s disease, showing
101 modest cognitive improvement after FUS [28]. However, this study did not induce BBBO or
102 investigate if there were any changes in amyloid or tau protein load.

103 In this Phase 1 clinical study (NCT04118764), we assessed the clinical feasibility and safety of
104 BBBO in six subjects with mild-to-moderate Alzheimer’s disease using a portable FUS system that
105 we developed and verified in preclinical studies [32–34]. A single 2-minute FUS sonication session
106 was performed per subject without a stereotaxic frame or a MR scanner. Real-time cavitation
107 monitoring was employed to measure the treatment dose and assess its capability of predicting
108 BBBO volume in the human brain. To our knowledge, this is the first report of real-time cavitation
109 mapping in the human brain using a portable FUS system. Neurological and biological effects of the
110 portable FUS system were evaluated by blood biomarker analysis, ^{18}F -Florbetapir PET scans, and
111 mini-mental state examination (MMSE).

112

113 **Results**

114 **Study Overview**

115 The primary objective of the study is to assess the safety and feasibility of FUS-induced BBBO in
116 Alzheimer's disease patients, using a portable, noninvasive FUS system. Secondary objectives
117 includes testing the feasibility of cavitation mapping and observing changes in ^{18}F -Florbetapir PET
118 and in blood biomarkers. Six Alzheimer's disease patients (2M/4F, age = 69.7 ± 7.2 yr) were enrolled
119 in a phase 1 trial under FDA and Columbia University IRB approval (NCT04118764) (Table 1).
120 Inclusion and exclusion criteria, including diagnosis of Alzheimer's disease, amyloid positivity on
121 ^{18}F -Florbetapir PET scan, and an MMSE score between 12 and 26, are listed in Table S1. Figure 2
122 presents the timeline of the clinical trial. All subjects underwent one session of FUS sonication and
123 had pre- and post-treatment scans, blood tests, and MMSE assessments.

124 **Portable NgFUS system allowed for efficient BBBO**

125 The target location was selected in a PET amyloid-positive region of the right frontal lobe, and the
126 FUS trajectory was determined by considering the beam incidence angle relative to the skull (Figure
127 3A). Skull insertion loss (i.e., attenuation), obtained from patient-specific acoustic simulations
128 (Figure 3B) and shown in Table 2, allowed us to adjust the sonication power to deliver a derated in
129 situ peak-negative pressure of 200 kPa. On the day of treatment, all subjects received a single FUS
130 treatment with microbubble administration (0.1 mL/kg) using the portable NgFUS system, while
131 seated in a medical recliner chair in an outpatient unit (Figure 3C). This process was guided by
132 neuronavigation (Figure 3D) and monitored by cavitation dose and mapping (Figure 3E). FUS was
133 deployed through a contact area with a diameter of less than 50 mm, which allowed for partial hair
134 shaving instead of complete head shaving (Figure S1). All sessions were uneventful and the average
135 treatment procedure time was 34.8 ± 10.7 min.

136 Five subjects underwent successful BBBO at the treated location in the frontal lobe as evidenced by
137 post-FUS T1-weighted MRI (Figure 4A), and the quantified contrast-enhanced volume, which
138 serves as a measure of BBBO volume, was 983 ± 626 mm³ (Figure 4C and 4D and Table 2). One
139 participant (subject 3) had no detectable opening (Figure S2), likely due to inadequate microbubble
140 administration caused by a syringe malfunction and patient movement resulting from not using the
141 head and chin rest. Subject 1 exhibited the largest opening volume of 2,013 mm³, which extended
142 to the left thalamus beyond the lateral ventricles while subject 4 exhibited the smallest opening
143 volume of 278 mm³. All of the openings from the 5 subjects were closed within 72 h, which was
144 confirmed by the follow-up scans on day 3 (Figure 4B). The opening and closing of the BBB were

145 confirmed by a neuro-radiologist, and the BBBO was quantified from the subtracted contrast-
146 enhanced T1-weighted MRI, as described in the Materials and Methods section.

147 **Safety evaluation**

148 There were no serious adverse events (SAEs) and no clinical changes after the treatments. One
149 subject (subject 1) had an adverse event (AE) including both mild skin erythema on day 0 (resolved
150 within 3 days) and asymptomatic cerebral edema with a superficial hemorrhagic component on day
151 3. MRI images showed an area of T2 fluid-attenuated inversion recovery (FLAIR) hyper-intensity
152 on day 3, most intense at the cortical targeted location but extending deeper (Figure S3), with
153 susceptibility-weighted imaging (SWI) hypo-intensity superficially within the same region (Figure
154 S4). The subject was asymptomatic and the MRI abnormalities were all resolved in follow-up scans
155 on day 15. Other subjects did not show abnormalities in the safety MR scans 3 days after the
156 treatment.

157 **Cavitation dose and map showed promising results for predicting the BBBO**

158 To monitor the safety and efficacy of the treatment, cavitation signal during sonication was observed.
159 Passive cavitation detection (PCD) with a single-element transducer was utilized to obtain cavitation
160 dose (CD) for subjects 1–4, while passive acoustic mapping (PAM) with a imaging array transducer
161 was employed for subjects 5 and 6 to obtain the 2-D cavitation maps.

162 Figures 5A–5C show the real-time cavitation dose monitoring results from subjects 1–4. For subjects
163 1, 2, and 4, ultraharmonic and broadband CDs increased after the microbubble injection ($t = 20$ – 30
164 s) and persisted until the end of the sonication ($t = 120$ s), indicating the cavitation activity of the
165 injected microbubbles (Figure 5A). On the other hand, for subject 3 which exhibited no detectable
166 opening, the increased CD was not sustained over time, resulting in a low cumulative CD (CCD).
167 The low cavitation energy for subject 3 is also evident in the spectrogram (Figure 5B). Across the
168 four subjects, the higher CCDs were detected with increasing BBBO volume (Figure 5C), resulting
169 in strong positive linear correlations ($R^2 > 0.9$, $p < 0.05$).

170 Figures 5D and 5E depict the real-time 2-D cavitation maps obtained by PAM and their
171 corresponding BBBO regions in MRI, respectively, from subjects 5 and 6. To our knowledge, this
172 is the first demonstration of 2-D transcranial PAM in the human brain. The cavitation map that shows
173 the spatial distribution of acoustic energy detected from microbubble activity (Figure 5D) roughly

174 matched with the BBBO location (Figure 5E); both the acoustic energy and BBBO locations were
175 shifted to the left side of the focus in subject 5, and aligned with the focus in subject 6. Compared to
176 subject 5, subject 6 showed approximately 12 dB higher averaged acoustic energy in the map and
177 exhibited a larger opening (278 mm^3 vs. 1262 mm^3). From the pixel-wise correlation analysis
178 between the PAM cavitation map and the BBBO volume observed in MRI, the area under the curve
179 (AUC) of the receiver operating characteristic (ROC) and precision-recall (PR) curves were
180 $\text{AUC}_{\text{ROC}}=0.8$ and $\text{AUC}_{\text{PR}}=0.7$, respectively, showing the potential of PAM for predicting BBBO
181 volume.

182 **Elevated blood biomarker levels correlated with BBBO size**

183 Both serum and serum-derived extracellular vesicle (EV) levels of biomarkers 3 days after FUS were
184 compared with the baseline levels obtained 1–2 hours prior to NgFUS for subjects 2–6. Subject 1’s
185 biomarker levels were not obtained due to improper handling of the blood specimen and were
186 excluded from the analysis. Figure 6 shows the correlation between BBBO volume and biomarker
187 levels for S100 β in serum, and A β 42, A β 42/A β 40, GFAP, Tau, and pT181 in EVs. Subjects with
188 larger opening volumes displayed elevated serum levels of S100 calcium-binding protein β (S100 β)
189 ($p < 0.05$), indicating compromised BBB integrity [35] (Figure 6A). Furthermore, we identified
190 several statistically-significant positive linear relationships between the opening size and the serum-
191 derived EV levels of Alzheimer’s disease-related proteins, while such relationships were not
192 observed with serum biomarker levels. Notably, glial fibrillary acidic protein (GFAP), Tau, and
193 phosphorylated-Tau 181 (pT181) fold-changes exhibited significant linear correlations ($p < 0.05$)
194 (Figure 6D–6F), while the correlations for A β 42 ($p = 0.062$) and the A β 42/A β 40 ratio ($p = 0.096$)
195 were not statistically significant (Figure 6B and 6C). There were no significant group-wise changes
196 possibly due to the large variation in BBBO volume (Figure S5).

197 **A modest decrease in asymmetry SUVR correlated with the size of BBBO and** 198 **cavitation dose**

199 Figure 7 shows the percent changes in standard uptake value ratio (SUVR) or asymmetry SUVR of
200 ^{18}F -Florbetapir compared to the baseline. Subject 3 was excluded due to the absence of BBBO.
201 Although there was no group-wise reduction in SUVR (Figure 7A–7C, Table 3), all subjects with
202 BBBO showed a modest reduction in asymmetry SUVR which assesses the SUVR in the treated

203 region compared to that of the contralateral region (Figure 7D–7F, Table 3). Specifically, asymmetry
204 values decreased by $1.47 \pm 0.77\%$ ($p=0.013$) in the frontal lobe and by $0.90 \pm 0.26\%$ ($p=0.001$) in the
205 hemisphere at the 2nd follow-up compared to the baseline. A non-significant linear relationship
206 ($R^2=0.69$, $p=0.08$) was measured between the BBBO volume and the 1st follow-up asymmetry
207 changes within the respective volumes (Figure 7G). A relationship of the asymmetry SUVR change
208 with CD was analyzed among subjects who exhibited BBBO with cavitation monitoring using a
209 single-element detector (subjects 1, 2 and 4). Although negative linear relationships were observed
210 between the 1st follow-up asymmetry changes and the CCDs (Figure 7H), these results should be
211 interpreted with caution due to the small sample size (Figure 7H). Changes in SUVR and asymmetry
212 values for each subject are listed in Table S2 and PET images are presented in Figure S2. SUVR
213 Changes in Centiloid units are shown in Figure S6 to enable standardized comparison with other
214 studies.

215 **A single BBBO treatment did not significantly alter cognitive function**

216 Comparing the baseline scores, the MMSE score decreased by 1.80 ± 2.71 among the five subjects
217 with BBBO and by 2.50 ± 2.93 among all six enrolled subjects, approximately 3 months after NgFUS.
218 When compared with the Alzheimer’s disease neuroimaging initiative (ADNI) database, subjects
219 with successful BBBO did not exhibit statistically different changes in MMSE over a similar time
220 frame ($p > 0.45$), indicating no cognitive changes due to FUS-induced BBBO (Table S3). Individual
221 MMSE scores are listed in Table S4.

222 **Targeting accuracy and precision**

223 Targeting of the FUS transducer during treatment was performed using a manual arm. The distance
224 and angular errors of manual transducer positioning were 5.7 ± 1.4 mm and $11.2 \pm 2.5^\circ$, respectively.
225 Mean absolute deviation and maximum distance of the subject motion during the 2-min treatment
226 were 0.3 ± 0.1 and 1.2 ± 0.2 mm when using a head and chin rest (subjects 4–6), and 2.3 mm and 9.4
227 mm without using the rest (subject 3) (Figure S7, Table 2). Distance between the centroid of the
228 BBBO and the simulated focus was 12.3 ± 6.1 mm, mostly along the FUS trajectory. There was no
229 consistent trend in the shift towards or away from the transducer, as it depended on the skull
230 properties and the selected treatment location for each subject.

231

232 **Discussion**

233 In this pilot study, we demonstrated the feasibility and safety of the portable FUS system with
234 cavitation monitoring for BBB permeability enhancement at the right frontal lobe in six Alzheimer's
235 disease patients. Five out of six subjects underwent localized BBBO which resolved within 72 h.
236 One AE occurred and resolved in 15 days, and no SAE was reported. No clinically significant
237 changes were observed in SUVR or cognitive test scores after FUS; however, the asymmetry SUVR
238 reduced modestly and exhibited a linear correlation with the BBBO volume. The CD demonstrated
239 correlations with the BBBO volume, blood biomarker level increase, and the asymmetry SUVR
240 decrease, proving the potential benefits of integrated cavitation monitoring to predict treatment
241 outcomes.

242 In clinical studies using MRgFUS, acoustic cavitation dose maps were generated by sonicating
243 dozens of subspots and mapping the measured cavitation dose to each subspot, assuming that the
244 received cavitation signals originated only from the focus, neglecting off-site cavitation [23,24,36].
245 In contrast, our portable FUS system provides a real-time 2-D cavitation map, offering not only off-
246 target cavitation imaging but also a more precise estimation of CD localized at the target. To our
247 knowledge, this is the first demonstration of 2-D PAM cavitation maps being obtained in the human
248 brain during BBBO. Cavitation mapping holds significant potential for enhancing both the safety
249 and efficacy of future treatments. By providing real-time visualization of cavitation activity, this
250 technology enables clinicians to immediately identify and mitigate any off-target effects, reducing
251 the risk of unintended damage to surrounding tissues. Furthermore, improved accuracy in estimating
252 the CD could result in more predictable and effective BBBO.

253 Although we aimed to deliver the same acoustic pressure at the brain target, the BBBO size varied
254 among the subjects from 278 mm³ to 2013 mm³. This variability could be attributed to the challenges
255 in estimation of skull-induced attenuation, which determined the FUS transmit power. The
256 attenuation estimates may have been affected by CT-MR registration errors in the acoustic
257 simulation (5–10 mm in distance and 1–16° in angle) that we identified at the conclusion of the trial.
258 Another factor may lie in the transducer positioning errors which caused discrepancies between the
259 trajectory used for the simulation and the achieved trajectory during treatment (Table 2). Further
260 analysis of the pressure estimation errors is presented in the Supplementary Discussion. The re-
261 estimated pressure map after correcting the errors and the trajectories showed higher acoustic energy

262 for larger opening cases (Figure S8A), with the most intense energy distribution in subject 1. The
263 re-estimated maximum pressure in the brain (Table S5) showed a linear relationship ($R^2 = 0.84$) with
264 the contrast-enhanced volume (Figure S8B), which may explain the variance in BBBO size across
265 the subjects and the AE in subject 1.

266 Five subjects showed contrast enhancement within an ellipsoidal volume along the FUS beam
267 trajectory (Figure 4C and 4D, and Movie S1) consistent with the cigar-shaped focus (Figure S8A).
268 Although the FUS focal volume included more white matter (WM) than gray matter (GM), the
269 opening volume exhibited similar proportions of GM and WM (Figure S9). The higher probability
270 of opening in GM than in WM was reported in our previous non-human primate (NHP) studies
271 [33,37,38], where GM exhibited increased susceptibility to BBBO relative to WM, indicated by
272 increased contrast enhancement on T1-weighted MRI. In this study, notable sulcal enhancements in
273 GM were observed (Figure 4A and Figures S10A and S10B). Additionally, the non-uniformly
274 distributed opening within the focal volume may be explained by the regional difference in vascular
275 density and tissue property, or increased ultrasound attenuation [37,39–42].

276 In subject 4, the contrast enhancement on MRI was found not only along the FUS trajectory from
277 the superior frontal cortex to the cingulate cortex, but also along the cingulate sulcus in the anterior-
278 posterior direction (indicated with white arrowheads in Figures 4A and 4C, and S9C). The sulcal
279 enhancement beyond the ellipsoidal focus might not indicate BBBO, because it extended
280 approximately 22 mm posterior from the focus while the focal size is only 6 mm wide. Instead, this
281 vessel-like extravasation of the contrast agent might have occurred through the vessel wall or the
282 perivascular space (PVS) that extends along the perforating vessels [43], indicating a potential
283 increase in permeability of the blood-meningeal barrier. A possible explanation might be that the
284 contrast agent entered the PVS through the disrupted BBB within the ellipsoidal focus and then
285 permeated posteriorly along the cingulate sulcus. This finding may be consistent not only with recent
286 preclinical studies on glymphatic clearance effect of microbubble-mediated FUS in rodents [44,45]
287 but also with clinical studies using MRgFUS [46,47]. These clinical studies also demonstrated
288 blood-meningeal barrier opening and glymphatic clearance in humans, reporting hyperintense linear
289 enhancement along the hippocampal fissure [47] and contrast accumulation in the subarachnoid
290 space at the frontal lobe [46] following BBBO.

291 The first possible reason for the BBBO failure in subject 3 is the delayed bolus injection of
292 compromised microbubbles due to the malfunction of the syringe/catheter system. The catheter was
293 blocked at the initial injection attempt, resulting in the pressurization inside the syringe and the
294 destruction of the microbubbles. Although the microbubble solution was eventually injected at $t =$
295 20 s after the start of sonication, the increases in CDs were minimal compared to other subjects
296 (Figures 5A and 5B). The second reason could be attributed to subject movement. The head and chin
297 rest were not used for this subject, resulting in the medial movement of ~9 mm during the 2-min
298 sonication, which was approximately 6–10 times larger than those of other subjects (Figure S7 and
299 Table 2). The subject movement (i.e., movement of the focus) might have compromised the localized
300 acoustic energy delivered, as evidenced by the reduced CDs at $t = 90$ s coinciding with the sudden
301 movement (gray arrows in both Figure 5A and Figure S7A).

302 In this study, statistically significant relationships between the opening size and harmonic,
303 ultraharmonic, and broadband cavitation energies were detected (Figure 5C), consistent with our
304 preclinical studies with mice and NHPs [33,48,49]. A recent study with MRgFUS in humans also
305 showed the correlation between the subharmonic acoustic emission and the contrast-enhanced T1-
306 weighted MR signal [23]. All subjects with BBBO showed overall increases in CD 20–30 s after the
307 microbubble bolus injection (Figures 5A and 5B), indicating the onset of microbubble cavitation
308 activity in the sonicated region. In some cases, the CD showed a high fluctuation before the major
309 increase (harmonic CD in subject 2 and ultraharmonic CD in subject 4) or did not increase even after
310 the flush (harmonic CD in subject 4). Compared to our preclinical studies with the same FUS
311 transducer [33,34] where flat CD was usually observed before the injection in NHPs fixed by a
312 stereotaxic frame, the baseline CD in this study was relatively unstable potentially due to motion. In
313 addition, fluctuations in CD can also result from tissues, small air-bubbles in the coupling gel, or the
314 membrane on the water cone [50]. The higher fluctuations observed in the harmonic and
315 ultraharmonic CD profiles can be attributed to the measurements based on peak amplitude, whereas
316 the broadband CD was determined by the averaged amplitude within a bandwidth. Additionally,
317 spectral leakage from narrowband (harmonic and ultraharmonic) signals into the broadband may
318 have occurred. An improved method for quantifying narrowband and broadband signals could be
319 employed in future studies [51].

320 Harmonic and ultraharmonic CDs are typically associated with stable cavitation, characterized by
321 the repetitive oscillation of microbubbles. Meanwhile, broadband CDs are more closely linked to

322 inertial cavitation, which occurs when microbubbles collapse, leading to more violent mechanical
323 effects. Due to these effects, monitoring of broadband CDs has been utilized to prevent tissue
324 damage in mice [52,53] and non-human primates [33]. Similarly, efforts have been made to
325 minimize the microbubble nonlinear behavior (i.e., subharmonic and ultraharmonic emissions) to
326 reduce the possibility of damage in rabbits [54,55]. In our clinical study, BBBO was achieved
327 without MRI-detectable damage in subjects 2 and 4, despite a 10–20 dB increase in ultraharmonic
328 and broadband CDs observed. This suggests that not only stable but also stable-inertial and inertial
329 cavitation was likely involved in facilitating BBBO [9,56]. Further studies are warranted to establish
330 safe thresholds for ultraharmonic and broadband CD levels that effectively induce BBBO without
331 causing tissue damage.

332 The reduction in SUVR was less pronounced in our study than in previous studies using an
333 implantable FUS device [27] or using an MRgFUS system [16–19,26]. This difference may be
334 attributed to the fact that we conducted a single session of treatment, while the prior studies involved
335 2–7 treatment sessions with larger treatment volumes. Nevertheless, we found significant decreases
336 in asymmetry at the 2nd follow-up (Figure 7E and 7F), indicating a lower A β accumulation rate or
337 elimination of amyloid in the treated side compared to the contralateral side. These asymmetry
338 changes after FUS are consistent with findings from prior studies [16–19,25–27]. In addition, this
339 lowered asymmetry SUVR across the treated frontal lobe and the hemisphere demonstrates the
340 potential of FUS to exert holistic therapeutic effects beyond the treated region. When measured
341 within the BBBO volumes in GM and WM (Figure 7D), the asymmetry did not show an apparent
342 group-wise reduction possibly due to the small and variable BBBO volumes across the subjects.
343 However, they correlated with the FUS treatment characteristics (i.e., BBBO size and CCDs)
344 (Figures 7G and 7H). A larger BBBO or a higher harmonic CCD was related to the reduced A β
345 accumulation in the treated region relative to the contralateral region. The observed decrease in
346 SUVR asymmetry may suggest the effectiveness of the targeted treatment, potentially indicating a
347 slowing or alteration in disease progression. Nevertheless, the small number of subjects in this pilot
348 study warrants further investigation with larger cohorts to confirm these preliminary findings.

349 Preclinical studies have reported improved cognitive function after FUS [14,57,58] and a clinical
350 study using MRgFUS has shown a cognitive improvement measured by the caregiver-administered
351 neuropsychiatric inventory (CGA-NPI) [17]. However, the majority of clinical studies so far have
352 reported non-significant changes in cognitive improvement following FUS-induced BBBO,

353 examined by MMSE and ADAS-cog, evidencing no worsening of cognitive decline due to FUS
354 [16,18,19]. Our MMSE results are also consistent with these findings.

355 A previous MRgFUS study reported significant increases in CSF T-Tau and CSF and plasma
356 neurofilament light chain levels 1 week after MRgFUS and associated the increases with the T2*
357 hypointensity findings in two patients [19]. In our study, although no group-wise changes in
358 biomarker levels were found, the BBBO volume was significantly correlated with the increased EV
359 levels of GFAP, Tau and pTau-181, 3 days after NgFUS without any abnormalities in MRI. The
360 absence of a significant correlation between changes in A β biomarker levels and BBBO volume
361 could be due to the small sample size or a weaker association with BBBO compared to other
362 biomarkers, given Meng et al.'s study, which also reported no significant changes in A β biomarker
363 levels [19]. The elevated levels of EV biomarkers indicate the release of proteins to the bloodstream
364 by FUS, consistent with sonobiopsy behavior noted in prior studies [59,60]. As the BBBO volume
365 also correlated with the reduced SUVR increase in the treated brain region, further investigation is
366 warranted to discover the potential of FUS for clearing Alzheimer's disease-related proteins from
367 the brain to the bloodstream. The overall increased correlation of BBBO volume with the proteins
368 in serum-derived EVs compared to serum levels alone indicates that EVs may be a more sensitive
369 diagnostic tool for biomarker detection as a result of FUS-mediated BBBO. Mitochondria or
370 endosome contamination was not accounted for in this study and may have influenced the absolute
371 biomarker levels. While this study captures biomarker changes at a single time-point, extending our
372 observations over multiple time-points would provide a more comprehensive understanding of
373 biomarker release attributed to FUS.

374 Despite the promising findings of the study reported herein, there are several limitations, including
375 a limited number of subjects, a single treatment at a single target location, inconsistency in BBBO
376 volume, and targeting errors. This was a single-arm phase I trial with only six subjects and no control
377 group. Despite the significant trends and differences observed in cavitation, biomarkers, and PET
378 analysis, the results of this study should be interpreted with caution due to the small number of
379 subjects. Furthermore, without a control group, the MMSE results might be influenced by placebo
380 effects and should be interpreted with caution. Additionally, since multiple treatments have proven
381 beneficial [26], evaluating the safety of regular NgFUS treatments is required. Future multi-arm
382 phase II/III trials will not only involve a larger number of subjects and incorporate sham groups but
383 will also include multiple NgFUS treatments to assess the safety of repeated sessions. Lastly, since

384 our study included only mild-to-moderate AD patients, our results may not necessarily be
385 generalizable to patients with lesser severity (pre-symptomatic), greater severity (severe disease), or
386 those with various medical comorbidities.

387 To achieve more consistent BBBO volume across subjects, precise transducer positioning and
388 accurate patient-specific simulations will be necessary in future studies. Based on our acoustic
389 simulations, maintaining a transducer positioning error less than 3–5 mm in distance and 4–6° in
390 angle is required to ensure an error margin of less than 10% in in-situ pressure. Robotics with
391 neuronavigation guidance could be utilized to minimize manual positioning errors, while patient-
392 specific fiducial markers could help reduce potential errors in registering the subject's head to a
393 virtual space. Moreover, we anticipate that the updated simulation pipeline will yield more accurate
394 skull-induced attenuation estimates, given the robust correlation observed between the re-estimated
395 attenuation and the resulting BBBO volume (Figure S8). Additionally, to further reduce inter-patient
396 variability, we plan to implement real-time closed-loop feedback controllers based on cavitation
397 metrics [61].

398 Furthermore, we plan to advance from our 2-D PAM to 3-D PAM using a matrix array probe,
399 providing more comprehensive volumetric cavitation information. Additionally, we will further
400 improve the mapping by employing skull-induced aberration correction.

401 Another limitation of our study is the small treated volume, considering that Alzheimer's disease
402 impacts broad regions of the brain [17,19]. To achieve more effective outcomes, our portable NgFUS
403 system could adopt a larger volume treatment approach by utilizing a robotic arm, similar to a pre-
404 clinical study by Leinenga et al [13]. In addition, a subject-specific hologram lens could be employed
405 for a larger and constant focal size across subjects [62].

406 **Conclusions**

407 The study presented herein demonstrates the safety and feasibility of transient and non-invasive
408 BBBO in patients with Alzheimer's disease using a portable NgFUS system. The BBBO volume
409 showed linear correlations with the treatment dose (i.e., CCDs), the elevated level of biomarkers in
410 serum-derived EVs, and the asymmetry SUVR changes. This low-cost and reliable technology may
411 facilitate wider adoption of FUS treatment at the point of care for not only Alzheimer's disease but
412 also for several other neurological disorders.

413 **Materials and Methods**

414 **Study Design**

415 This study was a phase 1 clinical trial (NCT04118764) of six subjects for evaluating the safety and
416 feasibility of NgFUS-mediated BBBO in patients diagnosed with mild-to-moderate Alzheimer's
417 disease. A power analysis prior to the trial showed that at least six subjects are needed to report a
418 result with a significance level of 0.05, a power of 0.95, and an effective size of 4 (e.g., to detect a
419 difference before and after FUS with a volume of 200 mm³ with a standard deviation of 50 mm³).
420 The study was approved by the FDA and the Institutional Review Board (IRB) at Columbia
421 University. After providing informed consent, participant eligibility was determined by the
422 neurologist on the study based on the MRI and 18F-florbetapir PET scans, the participant and family
423 interview, and clinical scales including MMSE, geriatric depression scale (GDS), and modified
424 Hachinski ischemia scale (MHIS) (Table S1). Out of the ten subjects screened, four subjects were
425 excluded due to low MMSE scores or the need for other medical treatment, and six subjects were
426 enrolled in the study. The timeline of the study is presented in Figure 2. All subjects had baseline
427 MRI and PET-CT scans 1–4 months before the treatment. For treatment planning, acoustic
428 simulations were performed to estimate the skull-induced ultrasound attenuation and determine the
429 FUS transducer output for each patient. On the day of treatment, the patient underwent one session
430 of FUS sonication and post-treatment MRI was obtained approximately 2 h after the sonication to
431 assess BBBO and safety. We aimed to establish a safety baseline with a single treatment session
432 before introducing more complex protocols involving multiple sessions. Follow-up MRI scans were
433 acquired 3 days after sonication to confirm BBB reinstatement and safety. Two follow-up PET scans
434 were performed 3 weeks and 3 months after FUS for all subjects except Subject 1, who underwent
435 follow-up PET scans at 3 days and 5 months, respectively. A 3-month follow-up period was deemed
436 sufficient to evaluate acute and mid-term side effects, assuming that long-term adverse effects due
437 to FUS were unlikely to occur more than 3 months post treatment. A follow-up MMSE was
438 administered on the day of the 2nd follow-up PET. The timeline for each subject is listed in Table S6.

439 **NgFUS System**

440 We used a single-element 250-kHz FUS transducer (H-231, Sonic Concepts) with a central opening,
441 with guidance achieved using a neuronavigation system (Brainsight; Rogue Research) which was
442 first tested in NHPs [32–34]. The FUS device was cleared by the FDA through an investigational

443 device exemption (IDE G180140) for a first-in-human study at Columbia University. The -6 dB
444 focal volume of the FUS beam was $6 \times 6 \times 49$ mm³ with an axially-elongated ellipsoidal shape. For
445 cavitation monitoring, either a single-element transducer for subjects 1–4 (Figure S11A) or a multi-
446 element imaging array transducer for subject 5 and 6 (Figure S11B) was coaxially inserted in the
447 central opening of the FUS transducer. A research ultrasound system (Vantage 256, Verasonics) was
448 used for cavitation map acquisition. The transducer specifications and experimental parameters are
449 listed in Table S7.

450 **Treatment Planning**

451 The target location was selected at an amyloid positive region in the right frontal lobe based on the
452 PET image. The initial FUS trajectory was determined by considering the focal size and the beam
453 incidence angle relative to the skull (Figure 3) for more efficient acoustic energy delivery [38].
454 Patient-specific numerical simulations were employed for estimating the skull insertion loss of the
455 acoustic pressure using the k-wave toolbox [63,64] and MATLAB (Figure 3B). Heterogeneous maps
456 of the skull density and sound speed were obtained from the CT image acquired during screening
457 (resolution: $0.6 \times 0.6 \times 1$ mm³, Biograph64 mCT, Siemens), where the maximum sound speed and
458 density were assumed to be $c = 4000$ m/s [65] and $\rho = 1850$ kg/m³ [66]. Skull absorption was also
459 modelled based on the CT image with a maximum absorption value of 0.68 dB/cm at the working
460 frequency, assuming a linear frequency dependency [66,67]. A 3-D acoustic pressure map was
461 obtained from the linear acoustic simulation with a grid size of $1 \times 1 \times 1$ mm³ (i.e., 6 points per
462 wavelength) and a time step of 52.5 μ s. The insertion loss α was determined by $\alpha = 1 - P_{\text{skull}}/P_{\text{freefield}}$,
463 where P_{skull} is the maximum pressure within the brain obtained from a simulated acoustic map with
464 skull insertion and $P_{\text{freefield}}$ is the maximum pressure from a simulated map without the skull. More
465 than 35 simulations were performed per subject considering the transducer positioning deviations
466 (i.e., ± 10 mm in distance and $\pm 10^\circ$ in angular deviation). The trajectory was also adjusted to avoid
467 a large deviation of the insertion loss based on the simulation, and was used for FUS treatment as
468 the planned trajectory. The estimated insertion loss along the planned trajectory (Table 2) was used
469 for adjusting the sonication power to deliver the derated *in situ* pressure of 200 kPa.

470 **FUS Sonication**

471 The dimensions of the portable FUS system required patients to have partial hair shaving at the right
472 frontal scalp for optimal acoustic coupling between the subject's head and the transducer (Figure

473 S1A). The subject's head was supported with the head and chin rest in a sitting position (Figure 3C),
474 and the anatomical registration to the neuronavigation system was performed based on the facial
475 landmarks (i.e., eyes, ears, and nose). The chin and head rest was used for subjects 2, 4, 5, and 6.
476 The FUS transducer was positioned with the neuronavigation guidance to place the acoustic focus
477 at the planned target in the right frontal lobe (Figure 3D). We determined the sonication parameters
478 based on our previous simulations and pre-clinical studies [32,33]. The sonication parameters were
479 as follows: derated peak-negative pressure, 200 kPa; mechanical index (MI), 0.4; center frequency,
480 0.25 MHz; pulse length, 10 ms; pulse repetition frequency, 2 Hz. treatment duration, 2 min.
481 Microbubbles (0.1 mL/kg, Definity, Lantheus) were intravenously injected as a bolus starting at 3 s
482 and finishing at 10–20 s after the start of the sonication, and followed with a saline flush.
483 Approximately 50–75% of the microbubble bolus was introduced into circulation at the time of the
484 flush due to the dead space within the catheter tubing. During the sonication, the frequency spectrum
485 and cavitation dose were monitored ($N=4$), and the cavitation map with ultrasound B-mode image
486 was also employed for the last two subjects ($N=2$) (Figure 3E).

487 **MRI and BBBO Quantification**

488 Baseline (screening), post-FUS (day 0, 2 hr after FUS), and follow-up (day 3) MRI scans were
489 acquired (Figure 2) using a 3-T MRI system (Signa Premier, GE). Safety MR scans were obtained
490 during all three MRI sessions without any MR-contrast agent and included T2-weighted, T2-FLAIR,
491 and SWI with parameters shown in Table S8. T1-weighted images with the gadolinium contrast
492 agent (0.2 mL/kg, Dotarem®) were acquired for the confirmation of BBB opening and closing on
493 day 0 and day 3, respectively. The post-contrast T1-weighted MRI was obtained 15–20 min after the
494 gadolinium injection for increased sensitivity to detect BBBO [68,69]. BBBO on day 0 and closing
495 on day 3 were confirmed by a neuro-radiologist.

496 The contrast-enhanced volume was quantified by subtracting the day-3 post-contrast T1-weighted
497 MRI from the day-0 post-contrast T1-weighted MRI and thresholding the subtracted image. The
498 threshold was automatically selected so that the mean intensity within the opening volume is
499 significantly greater than that of the surrounding region with a confidence level of 98% assuming
500 the intensity of the subtracted image follows a Gaussian distribution [34]. Evaluation of BBBO by
501 tissue types was performed using the brain segmentation methods described in the Supplementary
502 Methods.

503 **Blood Collection and Biomarker Measurement**

504 Blood was collected from patients both prior to BBBO and 3 days post-BBBO to assess blood-based
505 Alzheimer's disease biomarker detection as a result of FUS from both serum and serum-derived
506 EVs. All subjects had blood drawn immediately 1–2 hours prior to the treatment (i.e., baseline) and
507 3 days after treatment. Serum was isolated after centrifugation of whole blood at 9.4 rcf for 5 min at
508 4 °C, and serum-derived EVs were isolated using an exosome precipitation solution according to the
509 manufacturer's published protocol (ExoQuick, Systems Biosciences, Palo Alto, CA). A Luminex
510 multiplex assay was used to quantify proteins in serum and in isolated serum-derived EVs (Luminex
511 Corp., Austin, TX). Single pro-cartaplex kits (ThermoFisher Scientific) were purchased and
512 combined to make a custom multiplex panel for analysis. The biomarker levels of subject 1 were not
513 acquired properly because of mishandling of the blood specimen.

514 **PET/CT**

515 PET/CT scans (CT: no contrast, axial plane, 4 mm section thickness, 4mm section interval) were
516 acquired with a clinical PET scanner (Biograph64-mCT; Siemens) and with ¹⁸F-Florbetapir tracer
517 at 10mCi (Amyvid®; PETNET Solutions). PET/CT scans were acquired 32 to 107 days prior to
518 treatment, 3 to 29 days after treatment as the 1st follow-up time-point, and 82 to 164 days after
519 treatment as the 2nd follow-up time-point (Table S6). The A β load was quantified from PET scans
520 as SUVR, using the cerebellar GM as the reference region [70]. For region-specific amyloid analysis,
521 MRI and PET images were registered to the MNI space and automatically segmented by tissue types.
522 To investigate changes in A β from a localized region at the site of BBBO to extended regions, three
523 areas were analyzed: BBBO volumes in the GM and WM (SUVR_{BBBO*}), the treated right frontal
524 lobe (SUVR_{FL}), and the treated right hemisphere (SUVR_H). The asymmetry SUVR (Asym.SUVR)
525 was measured by dividing the average SUVR in the treated region by that in the contralateral region
526 to monitor the relative progression of A β . Changes in SUVR and asymmetry at the 1st and 2nd
527 follow-ups compared to baseline were quantified (Figure 7). SUVR in Centiloid scale was calculated
528 using established methods [71–73], in order to allow standardized comparison with other studies.
529 Details of PET analysis are presented in the Supplementary Methods.

530 **Cavitation Dose and Cavitation Mapping**

531 For cavitation monitoring, PCD was used for subjects 1–4 and PAM was employed for subjects 5
532 and 6. Device specification and parameters are listed in Table S7. The CD was obtained from the
533 3rd to 6th harmonic/ultraharmonic frequencies. We computed the CD with harmonic (CD_h),
534 ultraharmonic (CD_u), and broadband frequencies (CD_b) as described in the Supplementary Methods.
535 The CCD was obtained by summing the normalized CD acquired after the microbubble flush and
536 converting it to the logarithmic scale.

537 The cavitation map for each burst was reconstructed in real time from the 64-channel RF data by
538 using the coherence-factor-based PAM implemented on a GPU (RTX A6000, NVIDIA). The final
539 cavitation maps were obtained by averaging the acoustic energy maps for the bursts after the
540 microbubble injection and masking them with the segmented brain volumes obtained from the MR
541 images. More information on PAM implementation can be found in our previous study [34].

542 The BBBO volumes quantified in MR images were registered with the cavitation maps based on the
543 tracked coordinate of the focus by the neuronavigation system and also based on ultrasound B-mode
544 image that delineated the skin and skull; the registered B-mode (or cavitation map) and MRI slice
545 are presented in Figure S12. We evaluated the predictive capability of each pixel in the cavitation
546 image for detecting BBBO using the pixel-wise correlation. The AUC of ROC and PR curves were
547 calculated following the methods described in our previous study [34].

548 **Targeting Accuracy and Precision**

549 The planned target/trajectory of FUS was determined in the planning step before treatment and the
550 treated target/trajectory was sampled during the FUS sonication on the neuronavigation system.
551 Transducer positioning errors were measured by the distance and angle differences between the
552 planned and treated target trajectories to assess the accuracy in the manual placement of the
553 transducer. To evaluate the targeting accuracy of BBBO, the Euclidean distance between the BBBO
554 centroid and the simulated focus was measured for each subject. The subject movement was obtained
555 from the tracked location of the FUS focus which was recorded over time during the sonication by
556 the neuronavigation system.

557 **Post Hoc Simulation**

558 During the retrospective analysis of data, we found that there was a registration error between CT
559 and MR volumes (1–7 mm). Additionally, there were differences between the treated trajectory for

560 sonication and the planned trajectory for the acoustic simulation before treatment, due to the
561 transducer positioning error. We re-simulated the acoustic pressure fields with the corrected
562 registration and the trajectory. The pressure field (Figure S7), attenuation, and derated peak pressure
563 (Table S5) were obtained with the corrected trajectory and registration. The derated peak pressure \hat{P}
564 was calculated by $\hat{P} = P/(1 - \alpha) \cdot (1 - \hat{\alpha})$ where P is 200 kPa and α and $\hat{\alpha}$ are the original and the
565 newly obtained insertion loss values, respectively.

566 **Statistical Analysis**

567 Statistical analysis was performed in MATLAB (Mathworks). Linear regression analysis was used
568 to evaluate the correlations of the CCDs ($N=4$), biomarker levels ($N=5$), asymmetry SUVR increase,
569 and the simulated maximum pressure ($N=5$) with the contrast-enhanced volume, as well as the
570 correlation between the SUVR asymmetry and CCDs ($N=4$). R-squared and p values were obtained
571 from the regression for the statistical analysis. Pixel-wise correlation between the cavitation map
572 and the BBBO was measured by the AUC of ROC curve and the AUC of PR curve after combining
573 data sets from subject 5 and 6, as described in the previous study [34]. MMSE scores of the subjects
574 were compared with those of ADNI subjects by using unpaired t-test. Changes in SUVR and the
575 asymmetry between different time-points were analyzed using paired t-test.

576

577 **Abbreviations**

578	A β	Amyloid beta
579	AD	Alzheimer's disease
580	ADNI	Alzheimer's disease neuroimaging initiative
581	AE	Adverse event
582	BBB	Blood-brain barrier
583	BBBO	Blood-brain barrier opening
584	CCD	Cumulative cavitation dose
585	CGA-NPI	Caregiver-administered neuropsychiatric inventory
586	CT	Computed tomography
587	EV	Extracellular vesicle
588	FDA	U.S. Food and Drug Administration
589	FLAIR	Fluid-attenuated inversion recovery
590	FUS	Focused ultrasound
591	GM	Gray matter
592	GPU	Graphics processing unit
593	IRB	Institutional review board
594	MMSE	Mini-mental state examination
595	MRI	Magnetic resonance imaging

596	MR	Magnetic resonance
597	MRgFUS	Magnetic resonance-guided focused ultrasound
598	NHP	Non-human primate
599	NgFUS	Neuronavigation-guided FUS
600	PAM	Passive acoustic mapping
601	PCD	Passive cavitation detection
602	PET	Positron emission tomography
603	PR	Precision-recall
604	ROC	Receiver operating characteristic
605	SAE	Adverse event
606	SUVR	Standard uptake value ratio
607	SUVR _{BBBO*}	Standard uptake value ratio measured within BBBO volume in the gray and white
608	matter	
609	SUVR _{FL}	Standard uptake value ratio measured within the treated frontal lobe
610	SUVR _H	Standard uptake value ratio measured within the treated hemisphere
611	SWI	Susceptibility-weighted imaging

612

613 **Acknowledgments**

614 The authors wish to thank Maria F. Murillo, Alexander Berg, Rebecca L. Noel, and Nancy Kwon
615 for support and insightful discussion.

616

617 **Contributions**

618 ANP, EEK, and LSH initially developed the concept of the study;
619 SB, KL, RJ, SJG, OY, FNT, ANP, DK, LSH, and EEK conducted the FUS treatments;
620 LSH performed the neurological examinations;
621 SB processed and analyzed the cavitation, patient motion, and MRI data;
622 OY, KL, SJG, and FNT performed the numerical simulations;
623 KL and RJ processed and analyzed PET data;
624 AKS, AJB, SB, and FNT processed and analyzed blood biomarker data;
625 SB, RJ, SJG, KL, AJB, and EEK discussed and reviewed all the data;
626 KL, DK, ANP, and RJ assisted in patient recruitment;
627 ANP, KL, RJ, and SB prepared technical and regulatory documentation of the device;
628 EEK acquired funding and provided resources for the study as a principal investigator;
629 EEK and LSH supervised the clinical study;
630 SB wrote the original manuscript and visualized the data;
631 SB, KL, ANP, RJ, LSH, EEK, AJB, and SJG and edited the manuscript;

632 All authors reviewed and approved the final manuscript.

633

634 **Competing interests**

635 Some of the work presented herein is supported by patents optioned to Delsona Therapeutics, Inc.
636 where EEK serves as co-founder and scientific adviser. SB, ANP, RJ, KL, SJG, OY, FNT, DK,
637 AKS, AB, and LSH declare no conflict of interest.

638

639 **References**

- 640 1. Alzheimer's Association. 2022 Alzheimer's disease facts and figures. *Alzheimer's Dement.*
641 2022; 18: 1–118.
- 642 2. Budd Haeberlein S, Aisen PS, Barkhof F, et al. Two randomized phase 3 studies of
643 Aducanumab in early Alzheimer's disease. *Journal of Prevention of Alzheimer's Disease.*
644 2022; 9: 197–210.
- 645 3. van Dyck CH, Swanson CJ, Aisen P, et al. Lecanemab in Early Alzheimer's Disease. Vol.
646 388, *The New England Journal of Medicine*. Krause und Pachernegg GmbH; 2023.
- 647 4. Mintun M, Solomon P, Sims JR, et al. Donanemab in early symptomatic Alzheimer's disease:
648 Efficacy and safety in TRAILBLAZER-ALZ 2, a phase 3 randomized clinical trial. In:
649 Alzheimer's Association International Conference. Amsterdam;
- 650 5. Pardridge WM. Treatment of Alzheimer's disease and blood–brain barrier drug delivery.
651 *Pharmaceuticals*. 2020; 13: 1–25.
- 652 6. Banks WA, Terrell B, Farr SA, Robinson SM, Nonaka N, Morley JE. Passage of amyloid
653 protein antibody across the blood-brain barrier in a mouse model of Alzheimer's disease. Vol.
654 23, *Peptides*. 2002.
- 655 7. Pandit R, Chen L, Götz J. The blood-brain barrier: Physiology and strategies for drug delivery.
656 *Adv Drug Deliv Rev*. 2020; 165–166: 1–14.
- 657 8. McMahon D, O'Reilly MA, Hynynen K. Therapeutic agent delivery across the blood-brain
658 barrier using focused ultrasound. *Annu Rev Biomed Eng*. 2021; 23: 89–113.
- 659 9. Chen L, Cruz E, Oikari LE, Padmanabhan P, Song J, Götz J. Opportunities and challenges in
660 delivering biologics for Alzheimer's disease by low-intensity ultrasound. Vol. 189, *Advanced*
661 *Drug Delivery Reviews*. Elsevier B.V.; 2022.
- 662 10. Konofagou EE. Optimization of the ultrasound-induced blood-brain barrier opening.
663 *Theranostics*. 2012; 2: 1223–37.
- 664 11. Chen H, Brayman AA, Kreider W, Bailey MR, Matula TJ. Observations of translation and
665 jetting of ultrasound-activated microbubbles in mesenteric microvessels. *Ultrasound Med*
666 *Biol*. 2011; 37: 2139–48.

- 667 12. Kooiman K, Roovers S, Langeveld SAG, et al. Ultrasound-responsive cavitation nuclei for
668 therapy and drug delivery. *Ultrasound Med Biol*. 2020; 46: 1296–325.
- 669 13. Leinenga G, Bodea L, Schröder J, et al. Transcriptional signature in microglia isolated from
670 an Alzheimer’s disease mouse model treated with scanning ultrasound. *Bioeng Transl Med*.
671 2023; 8: e10329.
- 672 14. Karakatsani ME, Ji R, Murillo MF, et al. Focused ultrasound mitigates pathology and
673 improves spatial memory in Alzheimer’s mice and patients. *Theranostics* [Internet]. 2023; 13:
674 4102–20. Available at: <https://www.thno.org/v13p4102.htm>
- 675 15. Kline-Schoder AR, Noel RL, Phatnani H, Menon V, Konofagou EE. Focused Ultrasound-
676 Mediated Blood–Brain Barrier Opening Best Promotes Neuroimmunomodulation through
677 Brain Macrophage Redistribution. *Neuroglia*. 2023; 4: 141–57.
- 678 16. Lipsman N, Meng Y, Bethune AJ, et al. Blood-brain barrier opening in Alzheimer’s disease
679 using MR-guided focused ultrasound. *Nat Commun*. 2018; 9: 1–8.
- 680 17. Park SH, Baik K, Jeon S, Chang WS, Ye BS, Chang JW. Extensive frontal focused ultrasound
681 mediated blood-brain barrier opening for the treatment of Alzheimer’s disease: a proof-of-
682 concept study. *Transl Neurodegener*. 2021; 10.
- 683 18. Rezai AR, Ranjan M, Haut MW, et al. Focused ultrasound–mediated blood-brain barrier
684 opening in Alzheimer’s disease: long-term safety, imaging, and cognitive outcomes. *J*
685 *Neurosurg* [Internet]. 2022; 139: 275–83. Available at: [https://thejns.org/view/journals/j-
686 neurosurg/aop/article-10.3171-2022.9.JNS221565/article-10.3171-2022.9.JNS221565.xml](https://thejns.org/view/journals/j-neurosurg/aop/article-10.3171-2022.9.JNS221565/article-10.3171-2022.9.JNS221565.xml)
- 687 19. Meng Y, Goubran M, Rabin JS, et al. Blood–brain barrier opening of the default mode
688 network in Alzheimer’s disease with magnetic resonance-guided focused ultrasound. *Brain*.
689 2023; 146: 865–72.
- 690 20. Abrahao A, Meng Y, Llinas M, et al. First-in-human trial of blood–brain barrier opening in
691 amyotrophic lateral sclerosis using MR-guided focused ultrasound. *Nat Commun* [Internet].
692 2019; 10: 1–9. Available at: <http://dx.doi.org/10.1038/s41467-019-12426-9>
- 693 21. Gasca-Salas C, Fernández-Rodríguez B, Pineda-Pardo JA, et al. Blood-brain barrier opening
694 with focused ultrasound in Parkinson’s disease dementia. *Nat Commun*. 2021; 12.
- 695 22. Mainprize T, Lipsman N, Huang Y, et al. Blood-brain barrier opening in primary brain tumors
696 with non-invasive MR-guided focused ultrasound: A clinical safety and feasibility study. *Sci*
697 *Rep* [Internet]. 2019; 9: 1–7. Available at: <http://dx.doi.org/10.1038/s41598-018-36340-0>
- 698 23. Anastasiadis P, Gandhi D, Guo Y, et al. Localized blood-brain barrier opening in infiltrating
699 gliomas with MRI-guided acoustic emissions-controlled focused ultrasound. *Proc Natl Acad*
700 *Sci U S A*. 2021; 118.
- 701 24. Meng Y, Reilly RM, Pezo RC, et al. MR-guided focused ultrasound enhances delivery of
702 trastuzumab to Her2-positive brain metastases. *Sci Transl Med*. 2021; 13: eabj4011.
- 703 25. D’Haese PF, Ranjan M, Song A, et al. β -Amyloid plaque reduction in the hippocampus after
704 focused ultrasound-Induced blood–brain barrier opening in Alzheimer’s disease. *Front Hum*
705 *Neurosci*. 2020; 14.

- 706 26. Rezai AR, D’Haese P-F, Finomore V, et al. Ultrasound blood–brain barrier opening and
707 Aducanumab in Alzheimer’s disease. *New England Journal of Medicine* [Internet]. 2024;
708 390: 55–62. Available at: <http://www.nejm.org/doi/10.1056/NEJMoa2308719>
- 709 27. Epelbaum S, Burgos N, Canney M, et al. Pilot study of repeated blood-brain barrier disruption
710 in patients with mild Alzheimer’s disease with an implantable ultrasound device. *Alzheimers*
711 *Res Ther*. 2022; 14.
- 712 28. Jeong H, Song I-U, Chung Y-A, et al. Short-term efficacy of transcranial focused ultrasound
713 to the hippocampus in Alzheimer’s disease: A preliminary study. *J Pers Med* [Internet]. 2022;
714 12: 250. Available at: <https://www.mdpi.com/2075-4426/12/2/250>
- 715 29. Chen K-T, Chai W-Y, Lin C-J, et al. Neuronavigation-guided focused ultrasound for
716 transcranial blood-brain barrier opening and immunostimulation in brain tumors. *Sci Adv*.
717 2021; 7: eabd0772.
- 718 30. Chen K-T, Lin Y-J, Chai W-Y, et al. Neuronavigation-guided focused ultrasound (NaviFUS)
719 for transcranial blood-brain barrier opening in recurrent glioblastoma patients: clinical trial
720 protocol. *Ann Transl Med*. 2020; 8: 673–673.
- 721 31. Jeong H, Im JJ, Park JS, et al. A pilot clinical study of low-intensity transcranial focused
722 ultrasound in Alzheimer’s disease. *Ultrasonography*. 2021; 40: 512–9.
- 723 32. Pouliopoulos AN, Wu SY, Burgess MT, Karakatsani ME, Kamimura HAS, Konofagou EE.
724 A clinical system for non-invasive blood–brain barrier opening using a neuronavigation-
725 guided single-element focused ultrasound transducer. *Ultrasound Med Biol*. 2020; 46: 73–89.
- 726 33. Pouliopoulos AN, Kwon N, Jensen G, et al. Safety evaluation of a clinical focused ultrasound
727 system for neuronavigation guided blood-brain barrier opening in non-human primates. *Sci*
728 *Rep*. 2021; 11: 15043.
- 729 34. Bae S, Liu K, Pouliopoulos AN, Ji R, Konofagou EE. Real-time passive acoustic mapping
730 with enhanced spatial resolution in neuronavigation-guided focused ultrasound for blood-
731 brain barrier opening. *IEEE Trans Biomed Eng*. 2023; 70: 2874–85.
- 732 35. Marchi N, Cavaglia M, Fazio V, Bhudia S, Hallene K, Janigro D. Peripheral markers of blood-
733 brain barrier damage. Vol. 342, *Clinica Chimica Acta*. 2004.
- 734 36. Huang Y, Meng Y, Pople CB, et al. Cavitation feedback control of focused ultrasound blood-
735 brain barrier opening for drug delivery in patients with Parkinson’s disease. *Pharmaceutics*
736 [Internet]. 2022; 14: 2607. Available at: <https://www.mdpi.com/1999-4923/14/12/2607>
- 737 37. Wu SY, Sanchez CS, Samiotaki G, Buch A, Ferrera VP, Konofagou EE. Characterizing
738 focused-ultrasound mediated drug delivery to the heterogeneous primate brain in vivo with
739 acoustic monitoring. *Sci Rep*. 2016; 6.
- 740 38. Karakatsani MEM, Samiotaki GM, Downs ME, Ferrera VP, Konofagou EE. Targeting effects
741 on the volume of the focused ultrasound-Induced blood-brain barrier opening in nonhuman
742 primates in vivo. *IEEE Trans Ultrason Ferroelectr Freq Control*. 2017; 64: 798–810.
- 743 39. Fry FJ, Kossoff G, Eggleton RC, Dunn F. Threshold ultrasonic dosages for structural changes
744 in the mammalian brain. *J Acoust Soc Am*. 1970; 48: 1413–7.

- 745 40. Cavaglia M, Dombrowski SM, Drazba J, Vasanji A, Bokesch PM, Janigro D. Regional
746 variation in brain capillary density and vascular response to ischemia. *Brain Res.* 2001; 910:
747 81–93.
- 748 41. McDannold N, Arvanitis CD, Vykhodtseva N, Livingstone MS. Temporary disruption of the
749 blood-brain barrier by use of ultrasound and microbubbles: Safety and efficacy evaluation in
750 rhesus macaques. *Cancer Res.* 2012; 72: 3652–63.
- 751 42. Zhou H, Liu Y, Long X, et al. Feasibility of ultrasound-induced blood-brain barrier disruption
752 with a single-element transducer under three different frequencies in two non-human primates
753 in vivo: Case report. *J Neurosci Methods.* 2022; 365.
- 754 43. Wardlaw JM, Benveniste H, Nedergaard M, et al. Perivascular spaces in the brain: anatomy,
755 physiology and pathology. *Nat Rev Neurol.* 2020; 16: 137–53.
- 756 44. Ye D, Chen S, Liu Y, et al. Mechanically manipulating glymphatic transport by ultrasound
757 combined with microbubbles. *Proc Natl Acad Sci U S A.* 2023; 120.
- 758 45. Lee Y, Choi Y, Park EJ, et al. Improvement of glymphatic–lymphatic drainage of beta-
759 amyloid by focused ultrasound in Alzheimer’s disease model. *Sci Rep.* 2020; 10.
- 760 46. Meng Y, Abrahao A, Heyn CC, et al. Glymphatics visualization after focused ultrasound-
761 induced blood–brain barrier opening in humans. *Ann Neurol.* 2019; 86: 975–80.
- 762 47. Mehta RI, Carpenter JS, Mehta RI, Haut MW, Ranjan M. Blood-brain barrier opening with
763 MRI-guided focused ultrasound elicits meningeal venous permeability in humans with early
764 Alzheimer disease. *Radiology.* 2021; 298: 645–62.
- 765 48. Ji R, Karakatsani ME, Burgess M, Smith M, Murillo MF, Konofagou EE. Cavitation-
766 modulated inflammatory response following focused ultrasound blood-brain barrier opening.
767 *Journal of Controlled Release.* 2021; 337: 458–71.
- 768 49. Tung Y-S, Vlachos F, Feshitan JA, Borden MA, Konofagou EE. The mechanism of
769 interaction between focused ultrasound and microbubbles in blood-brain barrier opening in
770 mice. *J Acoust Soc Am.* 2011; 130: 3059–67.
- 771 50. Kamimura HAS, Flament J, Valette J, et al. Feedback control of microbubble cavitation for
772 ultrasound-mediated blood–brain barrier disruption in non-human primates under magnetic
773 resonance guidance. *Journal of Cerebral Blood Flow and Metabolism.* 2019; 39: 1191–203.
- 774 51. Lyka E, Coviello C, Kozick R, Coussios C-C. Sum-of-harmonics method for improved
775 narrowband and broadband signal quantification during passive monitoring of ultrasound
776 therapies. *J Acoust Soc Am.* 2016; 140: 741–54.
- 777 52. Sun T, Samiotaki G, Wang S, Acosta C, Chen CC, Konofagou EE. Acoustic cavitation-based
778 monitoring of the reversibility and permeability of ultrasound-induced blood-brain barrier
779 opening. *Phys Med Biol.* 2015; 60: 9079–94.
- 780 53. Xu S, Ye D, Wan L, et al. Correlation between brain tissue damage and inertial cavitation
781 dose quantified using passive cavitation imaging. *Ultrasound Med Biol [Internet].* 2019; 45:
782 2758–66. Available at: <https://linkinghub.elsevier.com/retrieve/pii/S0301562919306945>

- 783 54. O'Reilly MA, Hynynen K. Blood-brain barrier: Real-time feedback-controlled focused
784 ultrasound disruption by using an acoustic emissions-based controller. *Radiology*. 2012; 263:
785 96–106.
- 786 55. Jones RM, McMahon D, Hynynen K. Ultrafast three-dimensional microbubble imaging in
787 vivo predicts tissue damage volume distributions during nonthermal brain ablation.
788 *Theranostics*. 2020; 10: 7211–30.
- 789 56. Song JH, Moldovan A, Prentice P. Non-linear acoustic emissions from therapeutically driven
790 contrast agent microbubbles. *Ultrasound Med Biol*. 2019; 45: 2188–204.
- 791 57. Leinenga G, Götz J. Scanning ultrasound removes amyloid- β and restores memory in an
792 Alzheimer's disease mouse model. *Sci Transl Med*. 2015; 7: 278ra33.
- 793 58. Burgess A, Dubey S, Yeung S, et al. Alzheimer disease in a mouse model: MR imaging-
794 guided focused ultrasound targeted to the hippocampus opens the blood-brain barrier and
795 improves pathologic abnormalities and behavior. *Radiology*. 2014; 273: 736–45.
- 796 59. Meng Y, Pople CB, Suppiah S, et al. MR-guided focused ultrasound liquid biopsy enriches
797 circulating biomarkers in patients with brain tumors. *Neuro Oncol*. 2021; 23: 1789–97.
- 798 60. Pacia CP, Yuan J, Yue Y, et al. Focused ultrasound-mediated liquid biopsy in a tauopathy
799 mouse model. *Radiology*. 2023; 307.
- 800 61. Patel A, Schoen SJ, Arvanitis CD. Closed-loop spatial and temporal control of cavitation
801 activity with passive acoustic mapping. *IEEE Trans Biomed Eng*. 2019; 66: 2022–31.
- 802 62. Jiménez-Gambín S, Jiménez N, Pouliopoulos A, Benlloch JM, Konofagou E, Camarena F.
803 Acoustic holograms for bilateral blood-brain barrier opening in a mouse model. *IEEE Trans*
804 *Biomed Eng*. 2022; 69: 1359–68.
- 805 63. Treeby BE, Cox BT. k-Wave: MATLAB toolbox for the simulation and reconstruction of
806 photoacoustic wave fields. *J Biomed Opt*. 2010; 15: 021314.
- 807 64. Treeby BE, Jaros J, Rendell AP, Cox BT. Modeling nonlinear ultrasound propagation in
808 heterogeneous media with power law absorption using a k-space pseudospectral method. *J*
809 *Acoust Soc Am*. 2012; 131: 4324–36.
- 810 65. Marsac L, Chauvet D, la Greca R, et al. Ex vivo optimisation of a heterogeneous speed of
811 sound model of the human skull for non-invasive transcranial focused ultrasound at 1 MHz.
812 *International Journal of Hyperthermia*. 2017; 33: 635–45.
- 813 66. Pinton G, Aubry JF, Bossy E, Muller M, Pernot M, Tanter M. Attenuation, scattering, and
814 absorption of ultrasound in the skull bone. *Med Phys*. 2012; 39: 299–307.
- 815 67. Bossy E, Padilla F, Peyrin F, Laugier P. Three-dimensional simulation of ultrasound
816 propagation through trabecular bone structures measured by synchrotron microtomography.
817 *Phys Med Biol*. 2005; 50: 5545–56.
- 818 68. Israeli D, Tanne D, Daniels D, et al. The application of MRI for depiction of subtle blood
819 brain barrier disruption in stroke. *Int J Biol Sci [Internet]*. 2011; 7: 1–8. Available at:
820 <http://www.biolsci.org>
<http://www.biolsci.org>
- 821 69. Davies J, Siebenhandl-Wolff P, Tranquart F, Jones P, Evans P. Gadolinium:
822 pharmacokinetics and toxicity in humans and laboratory animals following contrast agent

- 823 administration. Vol. 96, Archives of Toxicology. Springer Science and Business Media
824 Deutschland GmbH; 2022.
- 825 70. Landau SM, Fero A, Baker SL, et al. Measurement of longitudinal β -amyloid change with
826 18F-florbetapir PET and standardized uptake value ratios. Journal of Nuclear Medicine. 2015;
827 56: 567–74.
- 828 71. Klein G, Delmar P, Voyle N, et al. Gantenerumab reduces amyloid- β plaques in patients with
829 prodromal to moderate Alzheimer’s disease: A PET substudy interim analysis. Vol. 11,
830 Alzheimer’s Research and Therapy. 2019.
- 831 72. Navitsky M, Joshi AD, Kennedy I, et al. Standardization of amyloid quantitation with
832 florbetapir standardized uptake value ratios to the Centiloid scale. Alzheimer’s and Dementia.
833 2018; 14: 1565–71.
- 834 73. Klunk WE, Koeppe RA, Price JC, et al. The Centiloid project: Standardizing quantitative
835 amyloid plaque estimation by PET. Alzheimer’s and Dementia [Internet]. 2015; 11: 1-15.e4.
836 Available at: <http://dx.doi.org/10.1016/j.jalz.2014.07.003>
- 837
- 838
- 839
- 840

841 **Table**

842

843 **Table I. Patient Characteristics**

Subject#	1	2	3	4	5	6
Age range	70-74	80-84	65-69	65-69	55-59	70-74
Sex	F	M	F	F	M	F
MMSE	18	20	15	21	24	15
GDS	1	1	2	1	0	0
MHIS	1	0	2	1	0	1

844 MMSE: Mini-Mental State Examination on the day of screening, GDS: Geriatric Depression Scale on the day
845 of screening, MHIS: Modified Hachinski Ischemia Scale

846

847

848 **Table 2. Summary of the treatment.**

Subject #	1	2	3	4	5	6
Contrast-enhanced volume (mm ³)	2013	414	0	951	278	1262
Skull-induced attenuation*	0.84	0.72	0.75	0.72	0.7	0.75
Procedure time** (min)	-	38	47	21	36	35
Transducer positioning errors† (mm, °)	-	4.7, 11.2	5.3, 13.0	4.3, 7.0	8.2, 14.5	5.8, 10.5
Subject movements†† (MAD, max) (mm)	-	-	2.3, 9.4	0.5, 1.5	0.25, 1.1	0.28, 0.96
Distance between the BBBO centroid and the simulated focus‡ (mm)	23.2	13.3	-	8.4	5.4	11.3

849 * Obtained by the acoustic simulation based on the planned target prior to the treatment.

850 ** Time duration for the subject sitting on the treatment chair; including anatomical registration for the
851 neuronavigation, targeting, sonication, and patient release.

852 † Distance (mm) and angle difference (°) between the planned trajectory and the actual trajectory during the
853 treatment.

854 †† Subject movement was measured by the mean absolute deviation (MAD) from its centroid and the
855 maximum distance (max) from the initial location.

856 ‡ Distance between the centroid of the BBBO and the estimated focal position in the simulated pressure
857 map

858

859 **Table 3. Changes in SUVR and asymmetry SUVR at the 1st and 2nd follow-up compared to**
860 **the baseline (mean±std)**

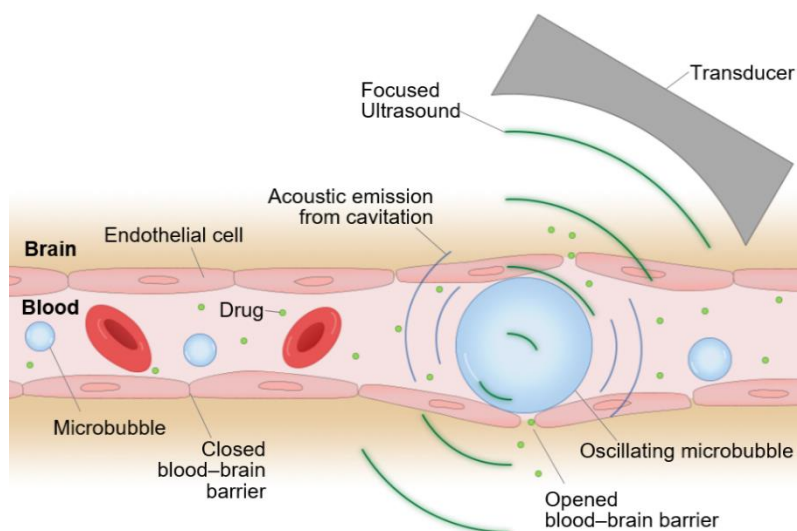
Region	ΔSUVR		ΔAsym.SUVR	
	1st F/U	2nd F/U	1st F/U	2nd F/U
BBBO*	-1.17±5.51, p=.66	5.05±7.20, p=.19	-1.67±5.09, p=.50	-0.68±1.05, p=.22
FL	1.97±5.51, p=.47	6.95±6.51, p=.076	-1.00±1.12, p=.12	-1.47±0.77, p=.013
H	1.43±5.73, p=.61	6.80±5.88, p=.061	-0.64±0.65, p=.092	-0.90±0.26, p=.001

861 SUVR: standard uptake value ratio, Asym.: asymmetry, BBBO*: blood-brain barrier opening in gray and white
862 matter, FL: frontal lobe, H: hemisphere, F/U: follow-up.

863 The 1st F/U and 2nd F/Us were 20±9 days and 103±30 days after focused ultrasound treatment, respectively.
864 Mean and standard deviations were calculated from 5 subjects with BBBO.

865

866 **Figure**

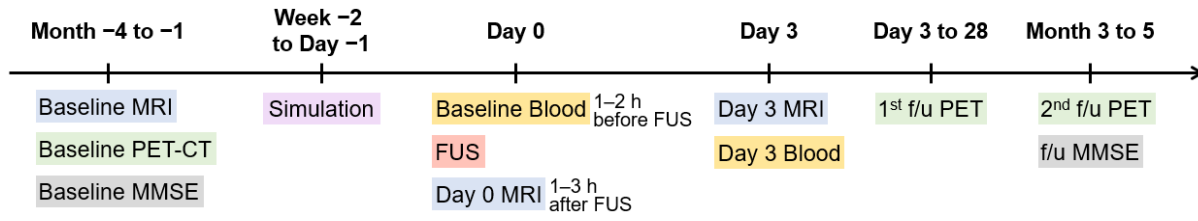


867

868 **Figure 1. Illustration of focused ultrasound (FUS)-induced blood-brain barrier (BBB) opening.**

869 Systemically administered microbubbles oscillate under localized FUS and transiently open the BBB for drug
870 delivery or immune-stimulation at the targeted brain tissue. Oscillating microbubbles emit acoustic cavitation
871 signals which can be used for treatment monitoring.

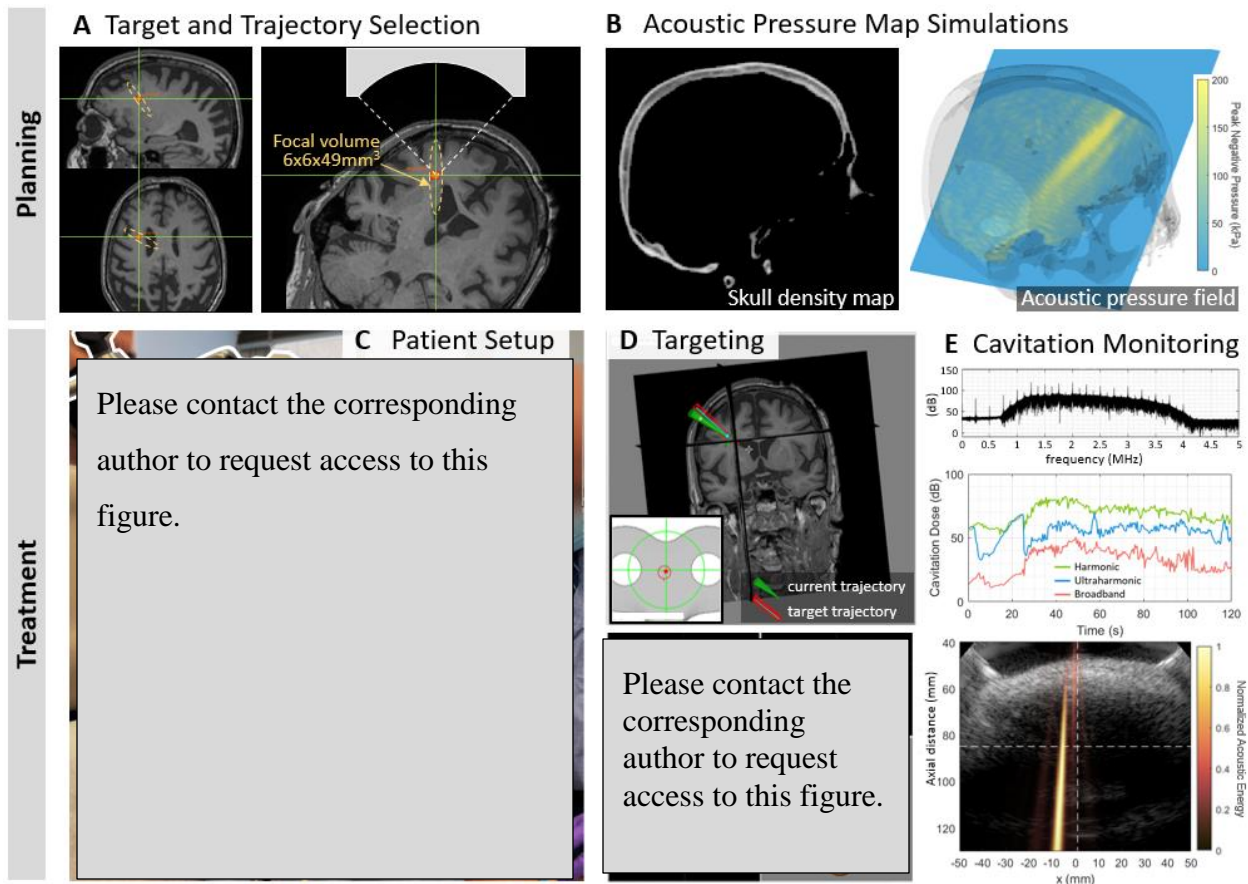
872



873

874 **Figure 2. Timeline of the clinical study**

875



876

877

878

879

880

881

882

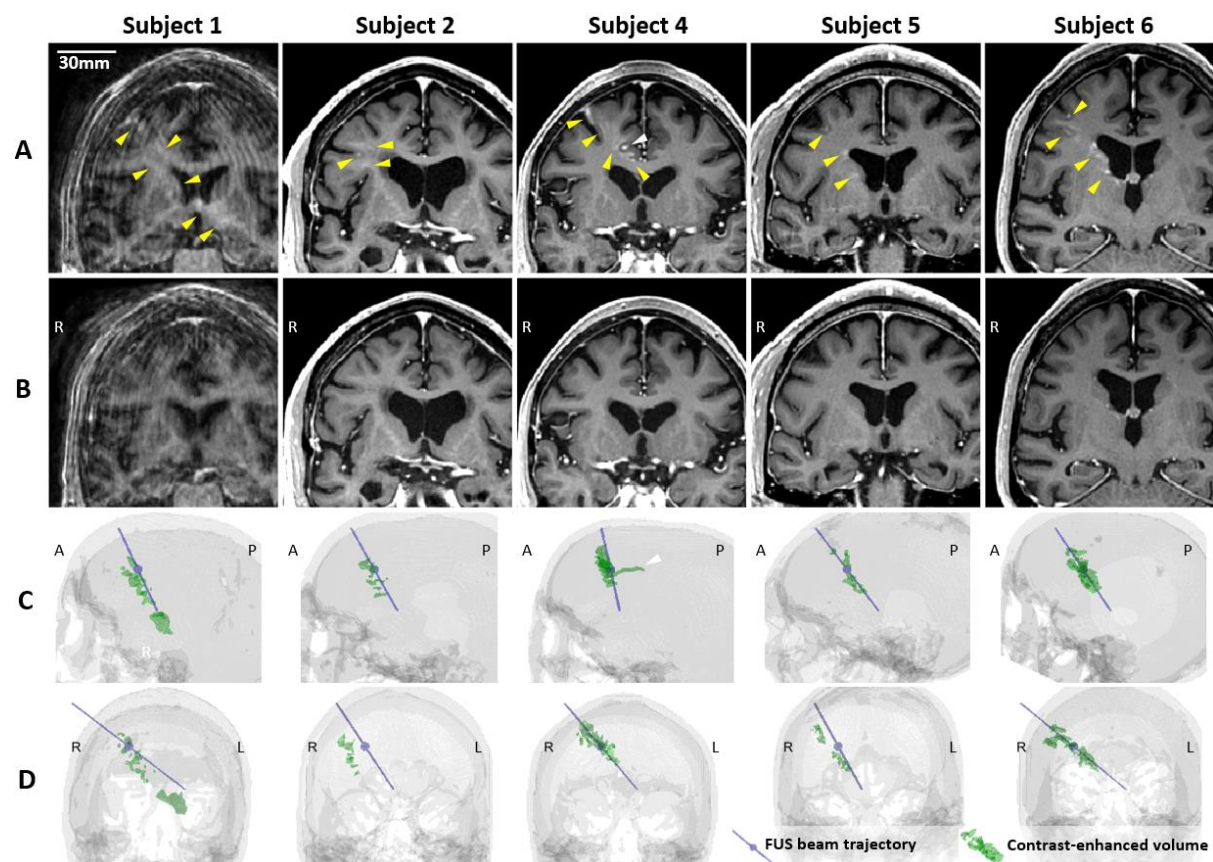
883

884

885

886

Figure 3. Portable NgFUS planning and treatment. (A) Selection of the target and the trajectory of the FUS beam. **(B)** Acoustic pressure map (right) obtained from simulations using CT image (left) for skull insertion loss estimation. **(C)** Subject undergoing the treatment session. The subject's head was supported and fixed by a head and chin rest. The FUS transducer with a coaxial single-element transducer (N=4) or a phased array transducer (N=2) was fixed with the metallic arm during the 2-min treatment. **(D)** Targeting with the real-time feedback of the neuronavigator. **(E)** Real-time cavitation monitoring with the frequency spectrum, cavitation dose, and cavitation energy map (color) with the B-mode image (grayscale) (from top to bottom). With PCD monitoring, only the frequency spectrum and cavitation dose were obtained. With PAM, a cavitation map was obtained as well as the spectrum and dose.



887

888

889

890

891

892

893

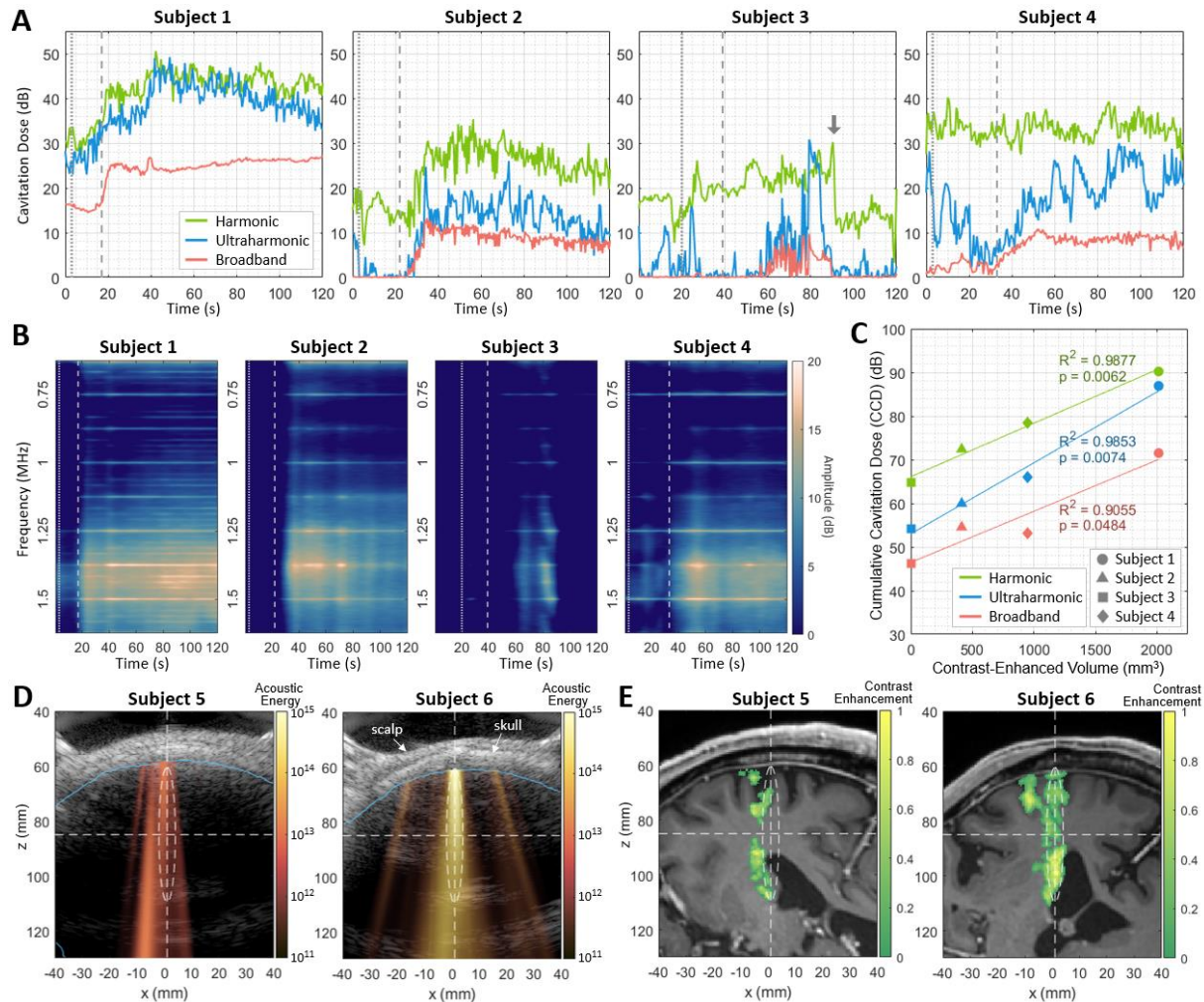
894

895

896

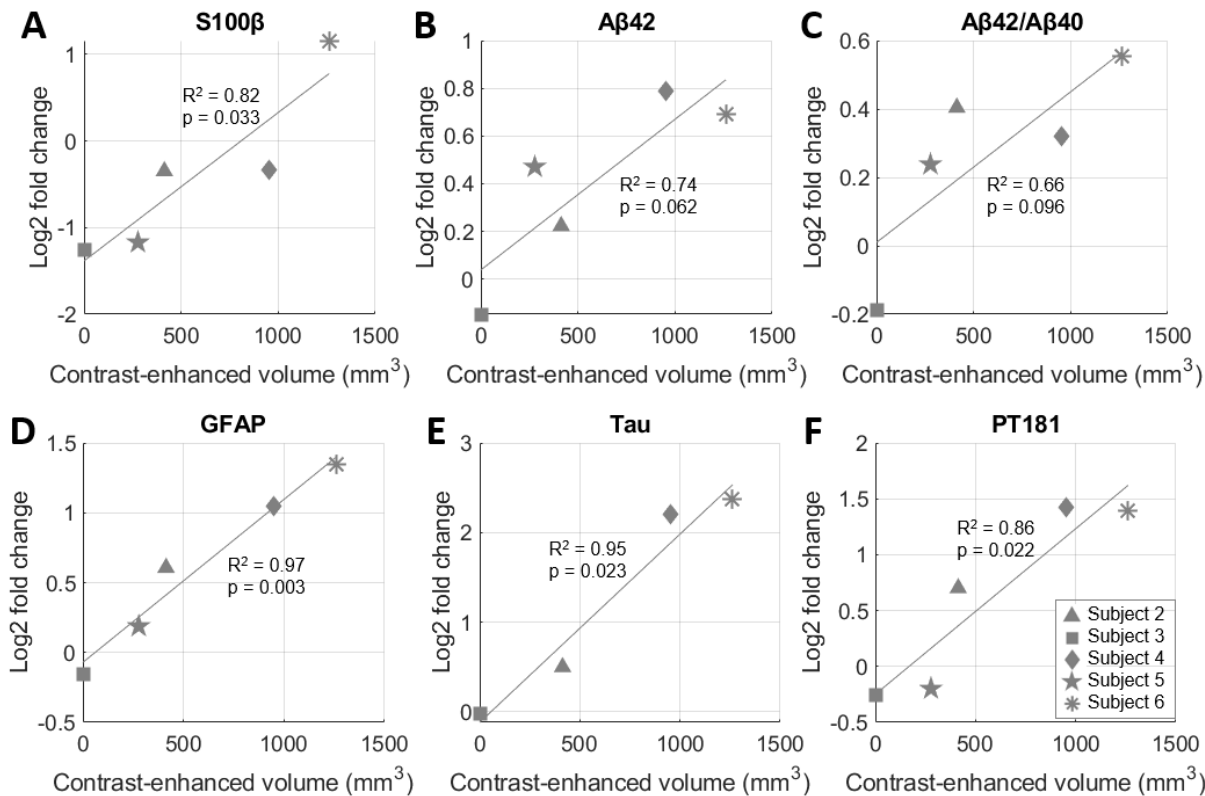
897

Figure 4. Blood-brain barrier (BBB) opening and closure confirmed by contrast-enhanced T1-weighted MRI. (A) Contrast enhancement indicating BBB opening in T₁-weighted MRI 2 hours after focused ultrasound (FUS) sonication. (B) Lack of contrast enhancement detected on follow-up T₁-weighted MRI confirmed BBB reinstatement on day 3. (C, D) The 3-dimensional (3-D) reconstruction of the FUS beam trajectory (blue line) and segmented contrast-enhanced volume (green) overlaid on the CT skull image (gray) in (C) the sagittal and (D) the coronal view. The maximum pressure point of the focus is denoted as a blue sphere on the blue line. The contrast-enhanced volume was well aligned with the FUS beam trajectory for subjects 4–6. For subjects 1 and 2, the opening was aligned with the trajectory in the sagittal plane (C) but approximately 10 mm off from the trajectory in the coronal plane (D). A video for 360° view of 3-D volumes is available online as Supplementary Movie 1.



898
899 **Figure 5. Real-time cavitation monitoring during focused ultrasound (FUS) treatment. (A)**
900 Harmonic, ultraharmonic, broadband cavitation doses (CDs) during the sonication. The CDs of subjects 1,
901 2, and 4 increased after the microbubble injection and flush and were sustained until the end of sonication.
902 In contrast, the CDs of subject 3, who did not exhibit successful BBBO, were unstable and exhibited a
903 sudden reduction at $t = 90$ s. The gray arrow indicates the moment of a sudden subject movement detected
904 (Supplementary Figure S7A). **(B)** Spectrograms displayed during the sonication showed the increased
905 cavitation signal in subjects 1, 2, and 4. Vertical dotted and dashed lines in (A) and (B) indicate the time of
906 the microbubble bolus injection and the subsequent saline flush, respectively. The amplitude in (B) was
907 normalized by the baseline broadband cavitation dose to better represent harmonic and ultraharmonic
908 components. **(C)** Positive correlation between the BBBO volume (i.e., contrast-enhanced volume) and the
909 cumulative CDs (CCDs) over time. **(D)** Cavitation map (color), which presents the distribution of acoustic
910 cavitation energy, is overlaid on the corresponding ultrasound B-mode image (gray) that shows the scalp
911 and the skull profiles. The brain region obtained from the registered MRI is marked as a blue line. **(E)**
912 Projected contrast-enhanced volume (color) overlaid on the MRI slice that is registered to the cavitation
913 map/B-mode image in (D). White dashed lines and ellipsoids in (D) and (E) show the focus of the FUS beam.

914



915

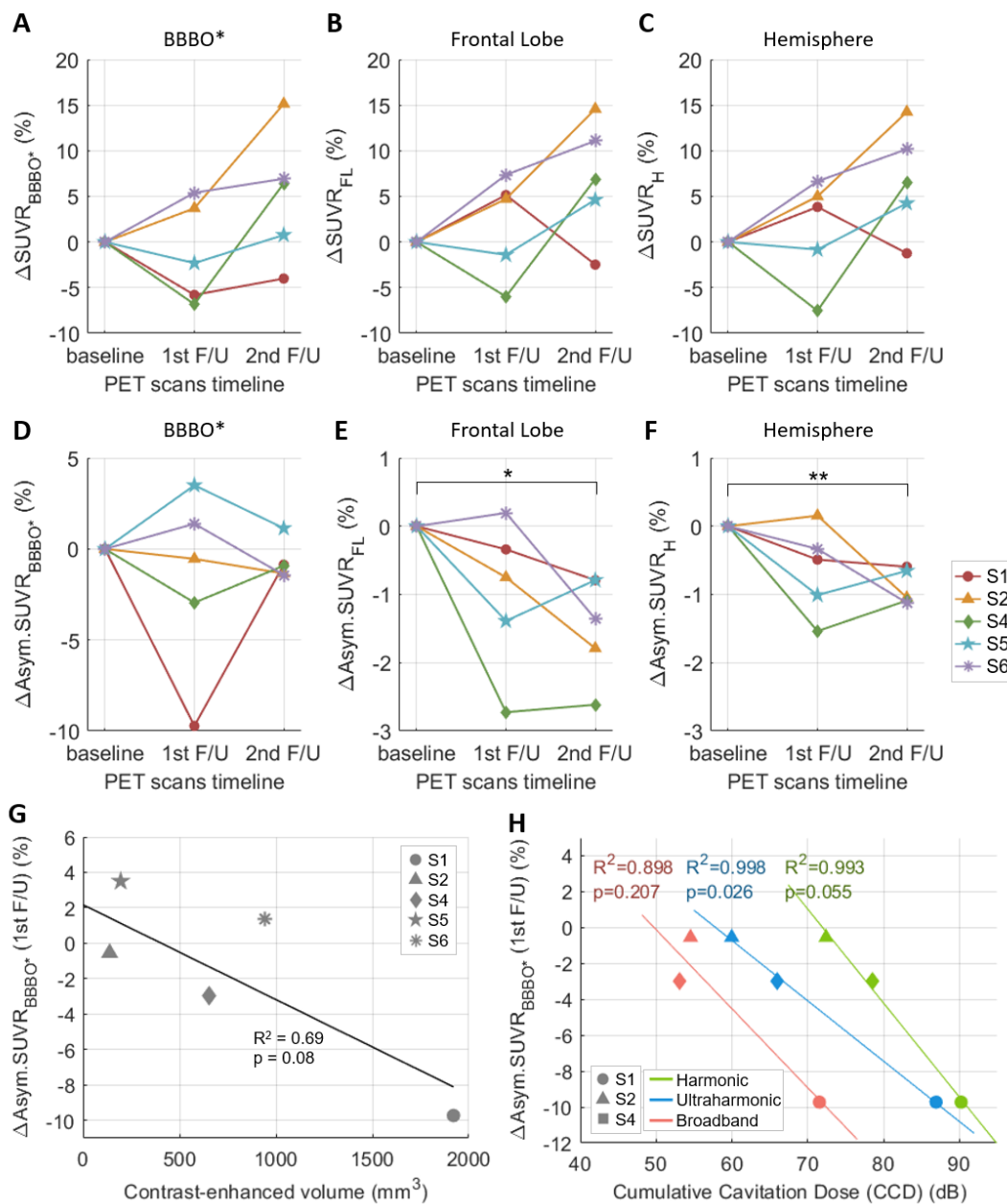
916

917

918

919

Figure 6. Correlation of blood-brain barrier opening (BBBO) volume and blood biomarker levels on day 3 after neuronavigation-guided FUS (NgFUS). A larger BBBO volume is associated with an increased log-fold change in biomarker concentration three days after treatment for **(A)** S100β in serum, **(B)** Aβ42, **(C)** Aβ42/Aβ40, **(D)** GFAP, **(E)** Tau, and, **(F)** pT181 in extracellular vesicles.



920

921 **Figure 7. Percent changes in the standard uptake value ratio (SUVR) and asymmetry SUVR**
 922 **of ^{18}F -Florbetapir and the correlation between the change in the asymmetry SUVR and the**
 923 **cumulative cavitation dose (CCD). (A–C) Percent changes in SUVR within the blood-brain barrier**
 924 **opening (BBBO) volume in the gray and white matter ($\Delta\text{SUVR}_{\text{BBBO}^*}$), the right frontal lobe ($\Delta\text{SUVR}_{\text{FL}}$), and**
 925 **the right hemisphere ($\Delta\text{SUVR}_{\text{H}}$), at the 1st and the 2nd follow-ups compared to the baseline. (D–F) Percent**
 926 **changes in asymmetry SUVR (Asym.SUVR) within the BBBO volume in the gray and white matter**
 927 **($\Delta\text{Asym.SUVR}_{\text{BBBO}^*}$), the right frontal lobe ($\Delta\text{Asym.SUVR}_{\text{FL}}$), and the right hemisphere ($\Delta\text{Asym.SUVR}_{\text{H}}$)**
 928 **compared to the baseline. Significant reduction in asymmetry values were found when measured within the**
 929 **(E) frontal lobe and (F) hemisphere regions. * $p < 0.05$, ** $p < 0.01$. (G) Linear correlation between the**
 930 **$\Delta\text{Asym.SUVR}_{\text{BBBO}^*}$ and the BBBO volume in the gray and white matter. (H) Linear correlations of**
 931 **$\Delta\text{Asym.SUVR}_{\text{BBBO}^*}$ with harmonic, ultraharmonic, broadband CCDs.**